O. Kislat, J. Zanger, T. Krummrein, P. Kutne, M. Aigner, Numerical Evaluation of a Micro Gas Turbine Range Extender Vehicle in Worldwide Harmonized Light Vehicles Test Cycle (WLTC) Scenarios, SAE Int. J. Elect. Veh. 12 (2023) 14-12-02-0008.

The original publication is available at
https://saemobilus.sae.org/content/14-12-02-0008/

Numerical Evaluation of a Micro Gas Turbine Range Extender Vehicle in Worldwide Harmonized Light Vehicles Test Cycle (WLTC) scenarios

Abstract

The idea of using a micro gas turbine (MGT) as range extender for Hybrid Electrical Vehicles (HEV) is discussed in literature for several years now. It is regarded from an experimental as well as from a numerical point of view, both indicating superior exhaust gas emissions and performance compared to piston engines. This is commonly shown applying a series consecutive New European Drive Cycles (NEDC). In 2017, however, the new approval procedure Worldwide harmonized Light vehicles Test Procedure (WLTP) was introduced with a more realistic drive cycle and also a specific test procedure for HEV. In this work, a drive cycle simulator is set up considering the essential vehicle components and incorporating a detailed model of the MGT's steady state as well as transient emission and performance behavior. The WLTP is applied to an MGT range extended HEV considering different operating strategies and vehicle configurations. Further, a procedure depleting a fully charged battery and a full fuel tank based on the Worldwide harmonized Light vehicles Test Cycle (WLTC) is carried out in comparison. The evaluation of the different operation concepts and missions shows very low exhaust gas emissions. A clear relation exists between the MGT load variations and the HEV's emission behavior and efficiency. It also shows that there are significant differences in the results either if the official WLTP is applied or the custom full range mission. These findings illuminate if the regarded procedures are suited to evaluate this range extender configuration and also provide information on future optimization targets for MGT HEVs.

Nomenclature

Alphanumeric Variables

C	capacity [kWh or l]
E	energy [kWh]
F	force [N]
G	gearing ratio [-]
M	emission mass [g/km or mg/km]
P	power [W]
c	emission concentration [mg/Nm3]
$\dot{m}$	mass flow [kg/s]
v	linear velocity [m/s]

Greek Variables

α	road inclination [°]
η	efficiency [%]
ω	angular velocity [rad/s]

Indices

aa	angular acceleration
ar	aerodynamic resistance
bat	battery
el	electric
exh	exhaust gas

hc	hill climb
i	emission component
la	linear acceleration
m	electric motor
p	(WLTC) phase
rr	rolling resistance
t	traction effort

Abbreviations

C30	Capstone® C30 micro gas turbine
CD	Charge Depletion
CS	Charge Sustaining
DLR	German Aerospace Center
HEV	Hybrid Electrical Vehicle
IUV	Inter Urban Vehicle
MGT	Micro Gas Turbine
NEDC	New European Drive Cycle
LHV	Lower Heating Value
LUT	Look Up Table
OPC	Operation Concept
SOC	State Of Charge
TIT	Turbine Inlet Temperature
TOT	Turbine Outlet Temperature
UF	Utility Factor
WLTP/WLTC	Worldwide harmonized Light vehicles Test Procedure/Cycle

Introduction

On September 16th, 2020, the European Union announced to tighten their goal for CO_2 reduction to 55 % compared to 1990. Road transport is one of the major contributors to global CO_2 emissions with the least reduction since 1990 [1] and is responsible for large amounts of inner-city air pollution, especially NO_X emissions [2]. Therefore, major steps have to be taken to reduce vehicle emissions. This is currently achieved by electrifying the vehicle power train. Replacing the traction engine by electric motors allows for locally emission-free driving. However, until battery capacity and charging times of pure electric vehicles (PEV) are adapted to long distance commuting [3], hybrid electric vehicles (HEV) can provide an interim solution for passenger cars [4].

The use of micro gas turbine based HEV is widely discussed in literature. Already in 1994, the development of a MGT based generator set is described for the use in HEV [5]. In recent years, several works evaluate the MGT HEV performance when applied to various driving scenarios and drive cycles. Yet, early numerical drive cycle evaluations have already been presented in 1998 by Leontopoulos et al. [6] comparing the performance of identical vehicles with a conventional diesel engine and a 50 kW prototype turbo generator set in US federal drive cycles. Also concepts of MGT hybrid passenger cars or hybrid buses are numerically investigated in custom drive cycles adapted from the NEDC by Capata et al. [7, 8] and Arefin [9], focusing on the issue of MGT efficiency and emissions. Several works discuss the application of Capstone® MGTs in HEV, such as investigating emission and operation strategy optimization of a 30 kW MGT for the New York M60 bus route [10] or comparing the performance of HEVs with 30 kW or 65 kW MGTs to a conventionally driven vehicle in the NEDC [11, 12]. Further works experimentally investigate the performance of a Capstone® C30 based MGT in automotive drive cycles, quantifying the effect of ambient conditions or air filtration requirements as well as investigating the impact of different operation strategies [13–15]. The common conclusion is that the micro gas turbine based HEV can hold emission and performance benefits compared to conventional vehicles. However, the applied driving cycles vary substantially between these works, and also the evaluation mode of the drive cycle differs. Karvountzis-Kontakiotis et al. [12] use 10 consecutive NEDCs to evaluate the MGT performance,

while Christodoulou et al. [11] consider the average demand of one cycle. Leontopoulos et al. [6] determine the test sequence by the range which can be achieved with a given battery and fuel capacity.

On September 1st, 2017, the Worldwide harmonized Light vehicles Test Procedure or WLTP was introduced as standard procedure for the approval of new vehicles in the European Union [16]. With the WLTP, the former NEDC is replaced by the WLTC. It is used as basis to determine the vehicle's performance with regard to approval-relevant parameters such as air pollutant emissions, fuel consumption and CO_2 emissions and the subsequent compliance with regulatory limits. It describes a specific test procedure that has to be followed regarding the sequence of cycles for different types of vehicles (ICE, HEV, Fuel-Cell-HEV) and the mode of calculation for the results, which is applied in the following study.

To address this procedure, a numerical drive cycle simulator is presented in this work to specifically evaluate the performance of MGTs as automotive range extenders. An Inter Urban Vehicle (IUV) of the DLR Next Generation Car Concepts [17] is simulated with an MGT range extender based on a 30 kW MGT [18], which has been previously experimentally characterized in detail [19]. The WLTP is applied to determine the performance of such a vehicle if assessed within the scope of a regulatory approval test. For comparison, a long-range evaluation is performed based on the full battery and fuel capacity of the vehicle. Different operation concepts for the MGT are tested in order to determine the effect of load set point variations on the exhaust gas emissions and fuel efficiency of the vehicle. The results allow to put the performance of an MGT based HEV into context of the current regulatory framework. Further they allow to determine the potential for optimization of MGTs when used in automotive applications.

Numerical Setup

The model for a generic HEV is composed in MATLAB SIMULINK®. Goal of the model is to replicate the essential components of the HEV, however focusing on a detailed representation of the MGT. The model is divided into sections for each component or calculation step. Model inputs are the base parameters of the car, the drive cycle in form of a velocity profile and the corresponding inclination of the route. The MGT model inputs are based on measurement data as presented in [19]. Data for steady state and transient operation such as start-up and shut-down are implemented. In each simulation cycle, the acting forces are calculated and, hence, the energy flow from and to the battery. If the MGT is running, the provided electric power and fuel consumption are considered, as well as exhaust gas emissions are calculated. In Appendix A, a detailed schematic of a full calculation cycle is shown. The inputs and components of the model are described in the following sections.

Vehicle Setup

The Inter Urban Vehicle (IUV) from the DLR Next Generation Car concept range is chosen as vehicle basis. The IUV is conceived as a comfortable long-distance traveling limousine with the capability to locally drive emission-free. It is designed as an electric vehicle with range extender. The main physical characteristics of the IUV are given in Table 1.

Table 1: Vehicle Parameters

Parameter	*Variable*	*Value*
frontal area	A_{front}	2.7 m^2
drag coefficient	c_{ad}	0.27
rolling resistance	c_{rr}	0.013
wheel diameter	D_{tire}	746 mm
gearing ratio	G	5.3
dry weight	m_{dry}	1574 kg
fuel capacity	C_{fuel}	40 l
battery capacity	C_{bat}	47.5 kWh
torque electric motor	$T_{t,\,max}$	280 Nm
power electric motor	$P_{t,\,max}$	95 kW

Traction Engine Model

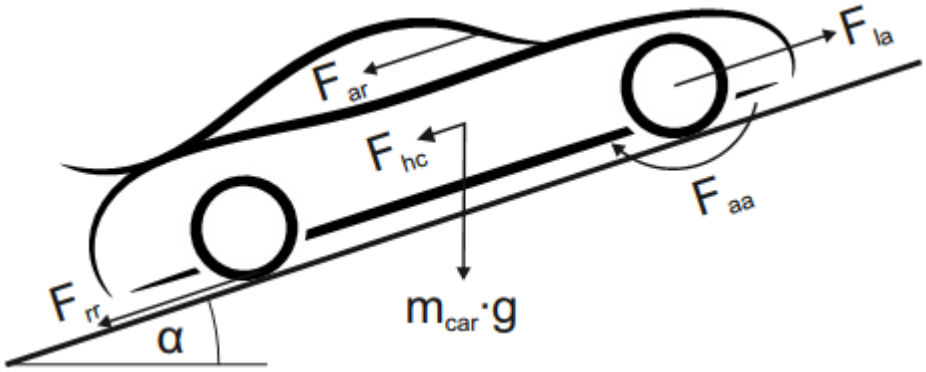

Figure 1: Schema of the modeled driving forces acting on the vehicle

The vehicle simulation is founded on the calculation of the tractive forces. The inertial force imposed by the electric engine in form of linear acceleration of the vehicle F_{la} is given by

$$F_{la} = m \cdot a \tag{1}$$

where m is the vehicle mass and a the acceleration [20], derived from the speed profile. The angular acceleration force F_{aa} of the wheels and motors is based on the torque inertia of the rotating parts. As no specific data is provided for the IUV, the angular acceleration force is estimated as a 5 % increase of F_{la}. This approach is also used in [12].

$$F_{aa} = 0.05 \cdot F_{la} \tag{2}$$

Further, there are resistance forces such as aerodynamic drag F_{ar} (Eq. (3)) and rolling resistance F_{rr} (Eq. (4)) or gravitational forces related to the road inclination F_{hc} (Eq. (5)) [20].

$$F_{ar} = \frac{1}{2} \cdot \rho_{air} \cdot v^2 \cdot c_{ad} \cdot A_{front} \tag{3}$$
$$F_{rr} = c_{rr} \cdot m \cdot g \cdot \cos \alpha \tag{4}$$
$$F_{hc} = m \cdot g \cdot \sin \alpha \tag{5}$$

Where v is the speed of the vehicle, c_{ad} the aerodynamic drag coefficient, A_{front} the frontal area of the car, c_{rr} the rolling resistance coefficient of the tires and α the inclination angle of the road. The tractive force F_t in Eq. (6) is the sum of the individual forces. From the tractive force the power P_t and torque T_t of the electric motor are calculated according to Eqs. (6) to (9). The rotation speed of the motor ω is calculated from the tire diameter D_{tire} and the gearing ratio G between traction motor and wheels.

$$F_t = F_{la} + F_{aa} + F_{ar} + F_{hc} \tag{6}$$
$$P_t = F_t \cdot v \tag{7}$$
$$\omega = \frac{2 \cdot v \cdot G}{D_{tire}} \tag{8}$$
$$T_t = \frac{P_t}{\omega} \tag{9}$$

A benefit of using electric motors to drive the wheels is that braking energy can be recovered using the electric motor as generator. Since the braking force of the electric motor is limited and friction braking is still required, it is assumed that on average 70 % of the braking power can be recuperated [21, 22]. Hence, the power of the electric motor P_m is calculated according to the following equations:

$$P_m = \frac{P_t}{\eta_m} \qquad \textit{for acceleration} \tag{10}$$
$$P_m = 0.7 \cdot P_t \cdot \eta_m \qquad \textit{for recuperation} \tag{11}$$

The efficiency of the electric motor $\eta_m(n,T)$ is given in form of a map as function of the rotation speed and torque of the motor, which is symmetric for acceleration and recuperation. The power requirement of auxiliary

consumers may vary significantly on ambient conditions or driver preferences [23]. In this study a constant demand of P_{aux} = 1000 W is assumed [22].

Battery Model

The battery is assumed as ideal. Internal losses, and a variation of output voltage depending on State Of Charge (SOC) are not considered. The energy consumption $E_{consume}$ which is subtracted from the energy content E_{bat} in each time step is calculated according to Eq. (12) with the MGT power input P_{MGT} considered negative. The SOC then is updated as stated in Eq. (13) with the battery capacity C_{bat}.

$$E_{consume} = \int_{t0}^{t1}(P_m + P_{aux} - P_{MGT})dt \tag{12}$$

$$SOC = \frac{E_{bat}}{C_{bat}} \cdot 100\% \tag{13}$$

The SOC is used to manage MGT start-up and shut-down. If the SOC drops below 15 % and fuel is available, the start-up sequence and the subsequent operation phase of the MGT are initiated. If the SOC increases above 85 % or, alternatively, the fuel tank is empty, the shut-down is initiated. In the latter case the vehicle will continue running until a SOC of 10 % is reached.

Micro Gas Turbine Model

Table 2: Base load readings of C30 MGT main parameters [19]

el. power	30 kW nominal
el. efficiency	25.5 %
rotational speed	96 krpm nominal
fuel consumption	2.7 g/s Kerosene
exhaust mass flow	291 g/s
NO_X emission	25.9 ppm @ 15 % O_2
CO emission	3.1 ppm @ 15 % O_2
CO_2 emission	4.54 Vol% @ 15 % O_2

The numerical model of the MGT is developed based on look up tables (LUT), which are derived from a detailed experimental investigation of a liquid fuel Capstone® C30 MGT [19]. The base load characteristics of the C30 are shown in Table 2. Model data is provided for steady state operation and transient maneuvers. In stationary power generation, MGTs are currently optimized for longevity in continuous operation, not for fast and frequent start up and shut down. Range extenders, however, require more frequent start-stop operation and, subsequently, the warm-up effects of the MGT have greater impact. Figure 2 shows fuel consumption and electric power and Figure 3 shows emissions during start-up. Over a span of six minutes, the values are remarkably elevated before converging to steady state level. Further, electric power is required to initially start up the MGT. After shut down further energy is required to cool down the MGT by rotating the turbine at 45 krpm for approximately 10 min. Taking this into consideration part load operation might be beneficial to reduce the amount of start-stop cycles. This is further addressed by the operation strategy in section *MGT Operation Strategy*.

MGT Start-Up Procedure

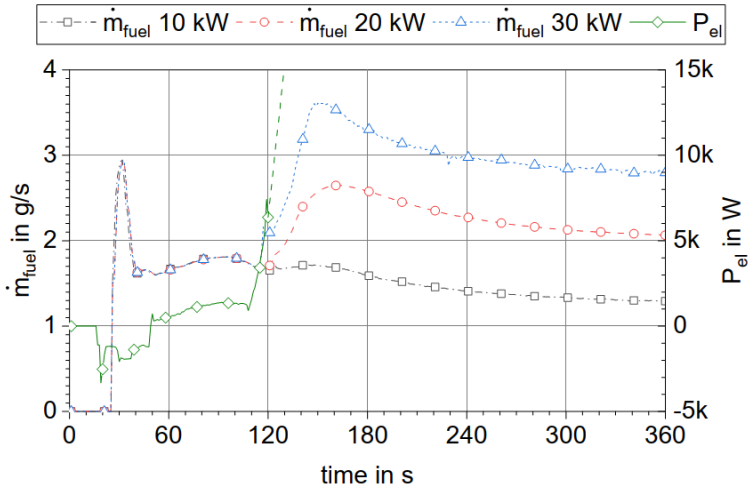

Figure 2: MGT start-up LUT for time dependent fuel mass flow and electric power

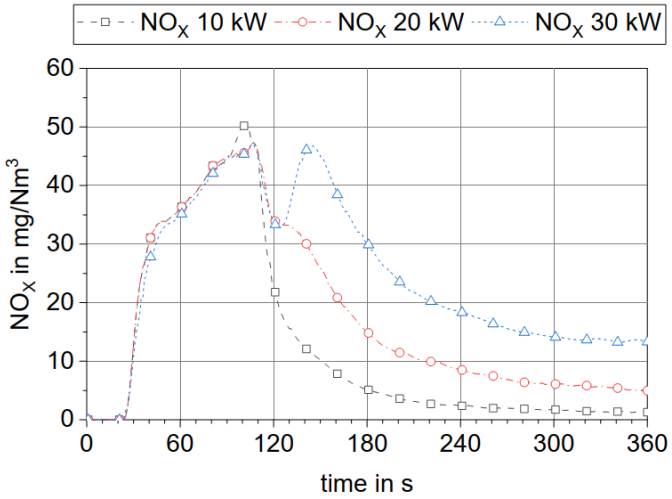

Figure 3: MGT start-up LUT for time dependent NO_X emissions

When the "MGT-run" command is triggered, a counter is started in the MGT section to differentiate between start-up and steady state operation. The start-up phase overall lasts 360 s. During this phase, time-resolved values are provided for fuel consumption, electric power (Figure 2) and emissions (Figure 3); here, the NOx trends are shown exemplarily. Emission concentrations c_i are converted to mass flows $\dot{m}_i$ according to Eq. (14) using the exhaust gas mass flow $\dot{m}_{exh}$ and density ρ_{exh}, which are also provided as transient table. Further, it can be seen that curves are recorded for three different load settings. The required data are interpolated in-between those trends. For the first 120 s, the curves are mostly overlapping since this part of the process is independent from the chosen load set-point. To provide a smooth interpolation between the trends, the transient table for electric power ends after 120 s (s. Figure 2) and subsequently the standard gradient for load changes as determined in [19] is applied. This is indicated by the dashed line in Figure 2.

$$\dot{m}_i = \frac{c_i \cdot \dot{m}_{exh}}{\rho_{exh}} \tag{14}$$

MGT Steady State Operation

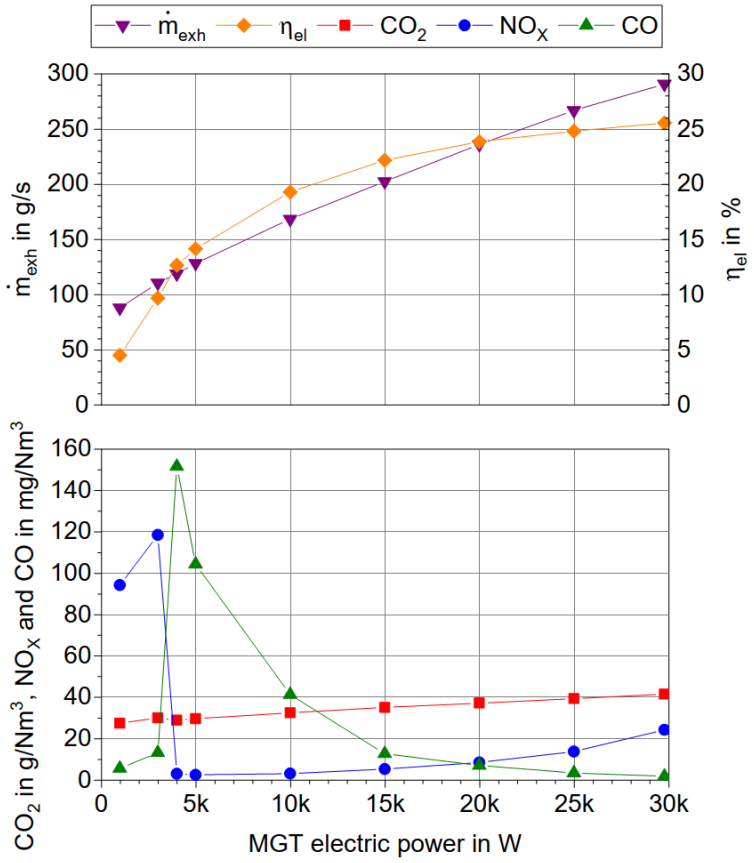

Figure 4: MGT steady state raw emissions, exhaust mass flow and electrical efficiency as a function of electrical power output

When the start-up time counter reaches 360 s, values are switched from the transient tables to the steady state values at the corresponding load set-point. For steady state operation, data points are provided for an MGT load range from 1 kW to 30 kW electrical power output. The model input parameters are displayed in the graphs of Figure 4. Raw emissions of CO_2, NO_X and CO are again presented as concentrations in the exhaust gas. Analogous to the transient data, they are converted to time-based emissions as shown in Eq. (14). Fuel consumption is calculated according to Eq. (15) from the MGT's electric efficiency, the current electric power output P_{MGT} and the fuel's *LHV* (43.2 MJ/kg).

$$\dot{m}_{fuel} = \frac{P_{el}}{\eta_{el}(P_{el}) \cdot LHV} \tag{15}$$

Further, the emissions and fuel consumption calculated according Eqs. (14) and (15) are converted to distance-based values with the WLTC speed profile of each time step. In particular, NO_X and CO emissions are converted to M_{NOx} and M_{CO} in *mg/km*, CO_2 to M_{CO2} in *g/km*. Further, fuel consumption is converted to *l*/100*km*.

Load changes of the MGT are realized by linear interpolation between the set points in the LUT. The transition speed is governed by the load gradient of the MGT. For the C30 the average load gradient has been determined to 900 W/s in both directions [19].

MGT Shutdown Procedure

The shut-down procedure is realized in a similar fashion as the start-up procedure. When the shutdown is initiated, a timer is started and MGT power output is switched to a transient table describing the cool-down procedure, where the shaft is rotated at 45 krpm. In the beginning, shaft rotation can be maintained from the residual heat in the recuperator, however, with decreasing temperatures, the speed has to be maintained by

drawing energy from the battery. Since at shut down the fuel supply is instantly cut by the shut off valve, no transient table is necessary. The same is assumed for pollutant emissions.

Driving Cycle and WLTP

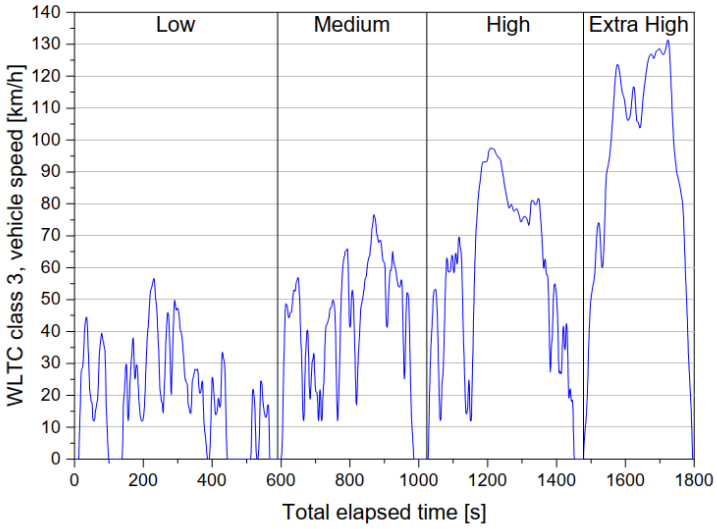

Figure 5: Velocity profile of the WLTC divided in the four phases (low, medium, high and extra high velocity) [16]

The WLTP is an extensive document, therefore this section highlights the most important requirements for modeling and evaluation. A full description can be found in the EU directive [16]. The drive cycle (WLTC) is implemented in form of a velocity profile as a function of time. It is the base input for the movement of the car. The cycle consists of four different phases that are concatenated according to the vehicle class. Each phase represents a different driving scenario, classified as Low, Medium, High and Extra High Speed Phase. HEVs are generally classified as class 3 vehicles which are tested in all four phases if the top speed is rated higher than 120 km/h. The full cycle lasts 30 min and 23.262 km with a maximum speed of 131.3 km/h. There is no road inclination implemented. Compared to the old NEDC, it features more phases with high acceleration and high speed driving. The test sequence for HEV is divided into two parts. The first part is called charge depletion (CD) test; it consists of consecutive full cycles during which the vehicle is operated in electric mode. The test starts with fully charged batteries and is concluded by the following two cycles: first, the transition cycle during which the combustion engine starts, and second, the confirmation cycle during which the charge is sustained by the combustion engine. In the second part of the test, after a cool-down phase, the vehicle performs one full cycle in charge sustaining (CS) mode, where the SOC is held at a constant level by the generator set. From the CD test a utility factor (UF) is derived according to eq. (16) for each phase p that is driven until the last phase t of the transition cycle. The UF is used to rate each emission component M_i and fuel consumption during CD and CS cycle as shown in Eq. (17). The distance driven until the end of each considered phase p is given by d_p and divided by the normalized distance d_n = 800 *km*. *C1* to *C10* are constants according to Table 3.

$$UF_p(d_p) = 1 - exp\left(-\left(\sum_{j=1}^{10} C_j \cdot \left(\frac{d_p}{d_n}\right)^j\right)\right) - \sum_{l=1}^{p-1} UF_l \quad (16)$$

$$M_{i,weighted} = \sum_{p=1}^{t}\left(UF_p \cdot M_{i,CD,p}\right) + \left(1 - \sum_{p=1}^{t} UF_p\right) \cdot M_{i,CS} \quad (17)$$

Table 3: Constants for UF calculation according to Eq. (16) [16]

C1	26.25	*C6*	60380.21
C2	-38.94	*C7*	-87517.16
C3	-631.05	*C8*	75513.77
C4	5964.83	*C9*	-35748.77
C5	-25094.60	*C10*	7154.94

The procedure requires that the test is performed in a standard operating concept (OPC) of the vehicle. If there are different concepts to choose from, the average of the best and worst constitute the test result. In this study, it is assumed that only one fixed OPC is implemented.

In comparison to the official approval test a second procedure is simulated. The IUV is capable of covering most of the typical daily commuting in pure electric driving mode [3]. The main purpose of the IUV, however, is long distance traveling. For this scenario, it is assumed that the vehicle's battery is completely charged and the fuel tank is filled at the starting point. The WLTC speed profile also serves as simulation basis, but the stop criterion is the maximum achievable range of the vehicle. This means that the fuel tank has to be empty and the SOC has to drop below a certain level at which the driver has to stop the vehicle. There is no distinction between CS and CD modes in this test, therefore no UF applies. As the WLTP postulates a revaluation of the UF calculation constants (Table 3) based on future technological developments and the use of real driving emissions instead of test bench measurements, this test can give an outlook towards this scenario. It is referred to as "full range" test in the following sections.

The final results of both tests will be considered in light of the regulatory limits provided by the EURO 6d norm [24]. An overview for petrol and gasoline engines is provided in Table 4. In preparation of the regulation EURO 7, position papers can be found already [25], promoting much lower, fuel-independent limits between 30 mg/km to 10 mg/km for NO_X and 200 mg/km to 100 mg/km for CO. With this background, a deeper assessment of the results is possible which may provide them with a long-term perspective.

Table 4: EURO 6d NO_X and CO emission limits [24]

	CO	*NO_X*
Diesel	500 mg/km	80 mg/km
Gasoline	1000 mg/km	60 mg/km

MGT Operation Strategy

The highest electrical efficiency of MGTs is given at base-load operation. Therefore, it appears obvious to run as much time on base-load as possible. In section *Micro Gas Turbine Model,* however, it is already indicated that the operation strategy of the MGT plays a more important role in automotive application compared to stationary power generation. Since the battery capacity is limited, the generator can only supply a limited amount of energy to the battery, depending on the consumption of the traction motor. In order to reduce the number of start-ups and shut-downs, it might be beneficial to operate in part load. Figure 2 and Figure 3 show that fuel consumption during a start-up to base-load is almost up to 1/3 higher than during stationary operation and that NO_X emissions surpass the stationary emissions by a factor of more than three. Additionally, as depicted in Figure 4, NO_X emissions increase with higher load, which might restrict operation due to regulatory NO_X limits. CO emissions in the contrary decrease with higher load, however, the limit is more liberal and allows for a wide operation window. To find the best trade-off for these boundary conditions, three operation strategies to manage the MGT load set point P_{MGT} shown in Table 5 are investigated in this paper.

Table 5: Overview of the simulated Operation Concepts

(A)	Constant Load Operation
(B)	Load Following Operation
(C)	SOC and Power Demand Based Operation

Constant Load Operation (A)

The most basic and static operation concept is to run the MGT at a predetermined constant load. For highest efficiency, constant base load operation is the best choice. But in order to find the best trade-off between efficiency and emissions, set-points from 5 kW to base-load at about 30 kW are simulated in 5 kW steps.

Load Following Operation (B)

The most dynamic option is to set the MGT load set-point instantly according to the traction motor power demand. Since the variation of the traction power demand can occur with higher gradients than MGT load changes, the actual power output of the MGT may react in a delayed manner. To avoid operation in disadvantageous load areas, a lower limit should be maintained. Limiting the minimum load also provides that the batteries are overall charged and not only the current SOC maintained. In this study, load following scenarios between 5 kW to 25 kW and base load are simulated.

SOC and Power Demand Based Operation (C)

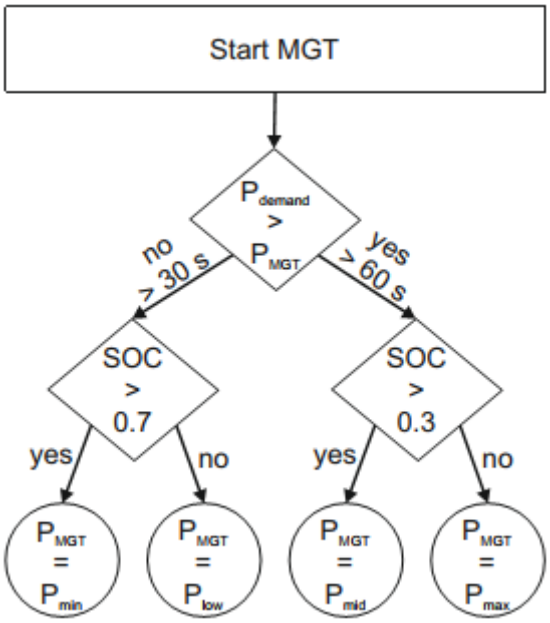

Figure 6: SOC and power demand OPC (C) load set-point decision chart

As a compromise, this operation strategy will switch MGT load between predefined set-points based on the power requirement of the traction motor and the current SOC of the batteries. Figure 6 shows the decision chart for the load set-point and Table 6 the simulated load set-point combinations. The first distinction is whether the power demand exceeds or falls below the current MGT output for a certain amount of time. For ongoing low average power demand with short acceleration peaks, it can be assumed that the car is operated in an urban area and the overall MGT power output is reduced. If the power demand remains on a high level for a prolonged amount of time, it is assumed to be related to high speed overland traveling and thus a higher power output level is chosen. MGT load is further differentiated according to the state of charge. If the power demand is low and the battery nearly charged, the range extender can be set to a minimum load or parking position P_{min} to avoid shut-down. For high power demand and low SOC, the power output of the MGT will be set to maximum P_{max} in order to avoid charge depletion. For low demand combined with low SOC or high demand with high SOC, intermediate settings P_{mid} or P_{low} are chosen. The SOC switch-points are kept constant.

Table 6: Simulated SOC and power demand-based operation MGT setpoint combinations

Index	P_{MGT} *kW*	$P_{MGT,mid}$ *kW*	$P_{MGT,low}$ *kW*	$P_{MGT,min}$ *kW*	*Index*	P_{MGT} *kW*	$P_{MGT,mid}$ *kW*	$P_{MGT,low}$ *kW*	$P_{MGT,min}$ *kW*
1	30	25	20	15	*26*	30	25	25	25
2	30	25	20	10	*27*	30	20	20	20
3	30	25	20	5	*28*	30	30	30	20
4	30	25	15	10	*29*	30	10	10	10
5	30	25	15	5	*30*	30	30	30	10
6	30	25	10	5	*31*	30	20	25	20
7	30	20	15	10	*32*	30	20	25	15
8	30	20	15	5	*33*	30	20	25	10

9	30	20	10	5
10	30	15	10	5
11	30	25	25	20
12	30	25	25	15
13	30	25	25	10
14	30	20	20	15
15	30	20	20	10
16	30	15	15	5
17	30	30	25	20
18	30	30	20	15
19	30	30	20	10
20	30	25	20	20
21	30	25	15	15
22	30	25	10	10
23	30	20	15	15
24	30	20	10	10
25	30	20	5	5

34	30	15	20	10
35	30	30	25	25
36	30	30	20	20
37	30	30	15	15
38	30	30	10	10
39	25	25	25	20
40	25	25	15	15
41	25	25	10	10
42	20	20	15	15
43	20	20	10	10
44	30	25	30	25
45	30	20	30	20
46	30	10	30	10
47	25	20	25	25

Results

In this section, the results of the simulated configurations are presented. The major aspects regarded in this section are exhaust gas emissions NO_x and CO, and fuel economy which is referred to in terms of CO_2 emission and fuel consumption in l/100 km.

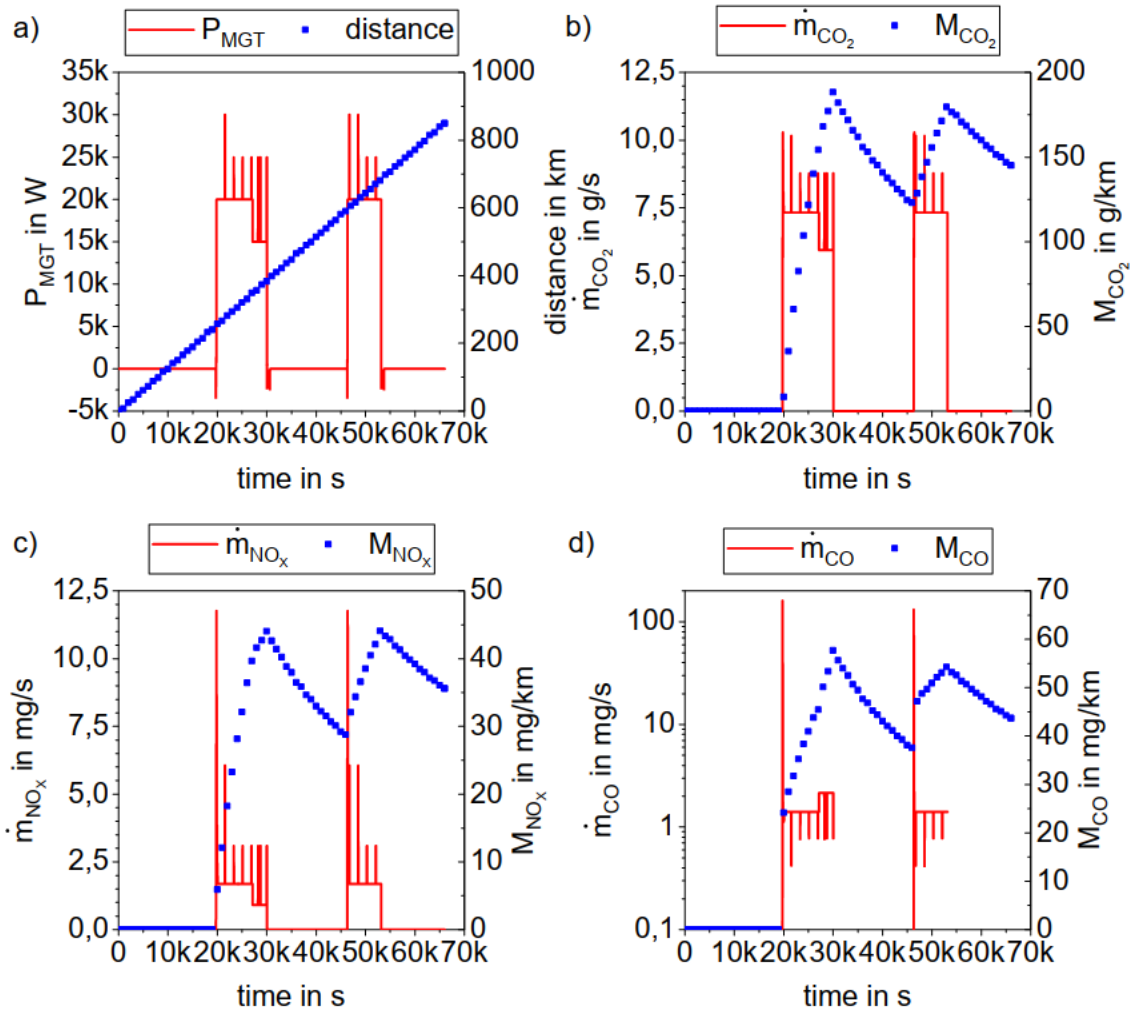

Figure 7: Illustration of the time trends of exhaust emissions, MGT power and distance during a full range test (Table 6, Index 1)

As an example for the simulation procedure, the time trends of these parameters during a full range test with the SOC and power demand based OPC (C) (Table 6, Index 1) are shown in Figure 7. Graph a) shows the covered distance and MGT power. The first 254 km are driven in pure electric mode before the MGT starts up. In total, the MGT runs twice during this test. The first run lasts 3 h and the second approximately 2 h. MGT power varies between 15 kW and 30 kW. The graphs in Figure 7 b), c) and d) show the instantaneous emissions of NO_X and CO in mg/s and CO_2 in g/s. Further the resulting accumulated NO_X and CO emission masses M_i over the course of the test in mg(NO_X,CO)/km or g(CO_2)/km are shown. In the following evaluation the final emission values at the end of the test are considered as well as the maximum value throughout the test; in order to monitor if the vehicle is emission-compliant during the entire test.

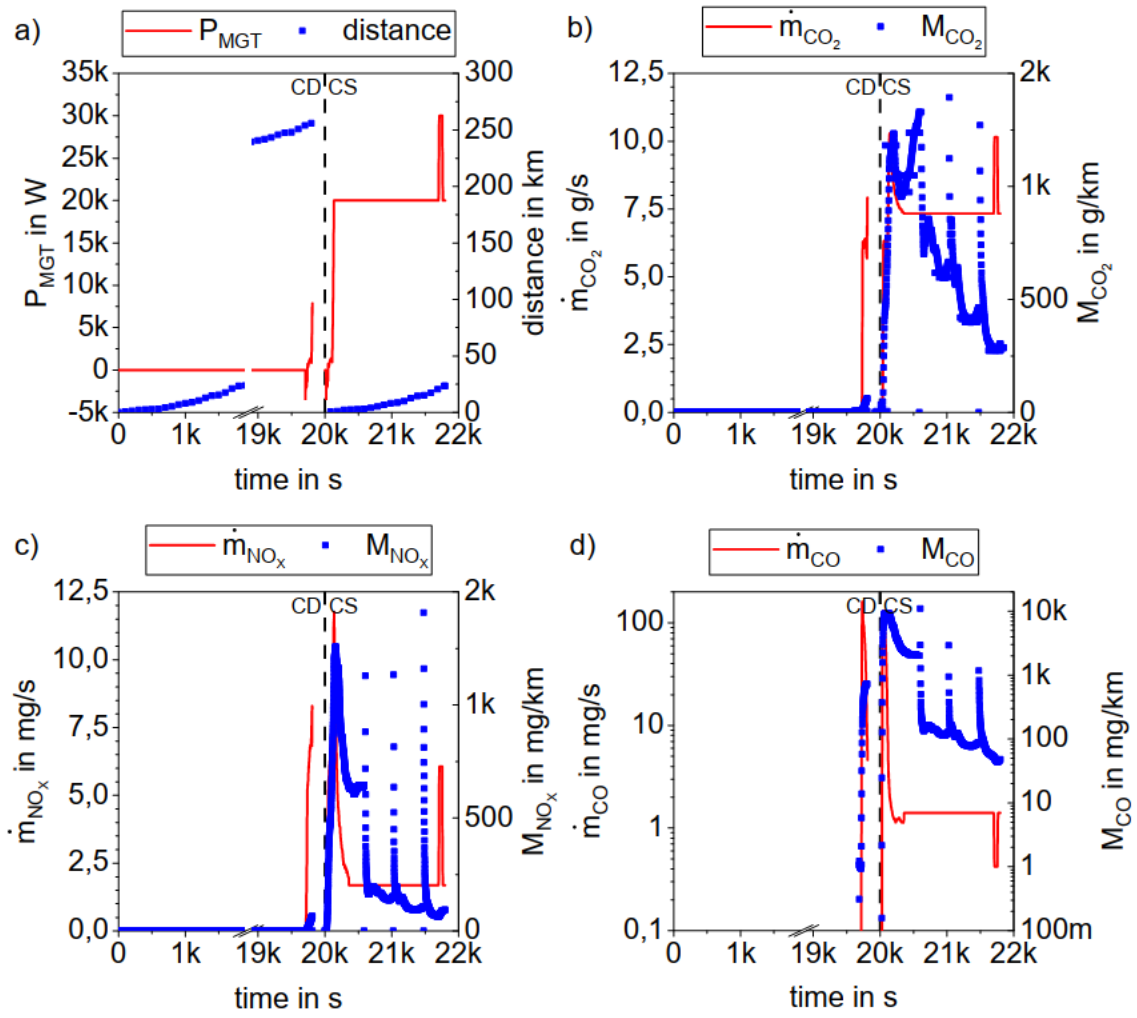

Figure 8: Illustration of the time trends of exhaust emissions, MGT power and distance during a WLTP test (Table 6, Index 1)

Figure 8 shows the trend of the same operation concept (Table 6, Index 1) tested according to the WLTP. The first 20000 s comprise the CD test in pure electric mode, with the MGT starting during the last cycle. Since the pure electric range of the CD test foremost depends on the battery capacity, it is the same for all operation concepts and hence $\sum UF_p = 0.98101$ is the same for all cases as well. From Eq. (17) it can then be derived that only 2 % of the emissions during the CS cycle are counted. From 20000 s onward, the CS cycle is displayed. Graph a) again shows the traveled distance and MGT power. Since CD and CS test are evaluated separately

(Eq. (17)), the accumulated distance restarts with the CS test. Graphs b), c) and d) again show CO_2, NO_X and CO emissions. However, as required by the test procedure, the emission masses are integrated over each phase of the regarded cycles individually. This leads to the spikes at the beginning of each phase when the traveled distance resets. For evaluation, the final emission mass values M_i at the end of each phase are decisive.

Constant Load Operation (A)

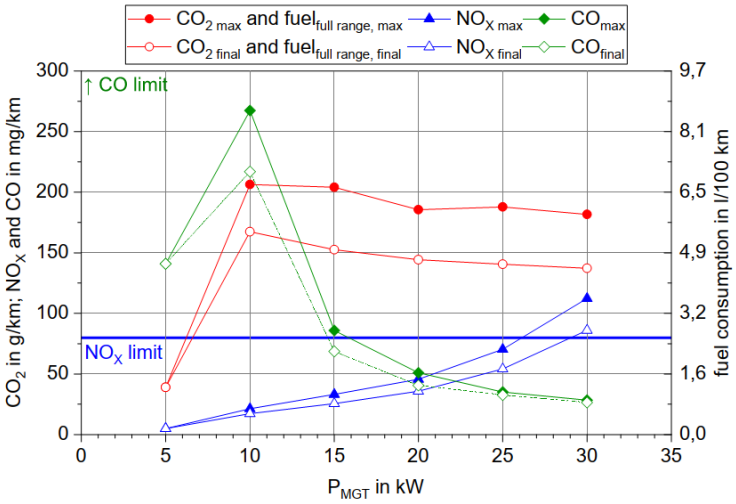

Figure 9: Range and emission results for the full range test with constant load OPC (A) dependent on MGT load setpoint

Figure 9 shows the results for NO_X, CO and CO_2 as well as the corresponding fuel consumption of the full range test with constant load OPC (A) plotted as function of the MGT load set point. For each parameter, the maximum value during the test and the final result at the end of the test are shown. The trends are monotonous except for 5 kW MGT load, which marks a drop in all trends. This results from the low MGT power which is not sufficient to sustain the battery charge for the given velocity profile. Hence the test is aborted due to the SOC dropping below 10 % before the fuel tank is depleted. For the remaining load set-points, CO_2 emissions vary around 150 g/km, slightly decreasing with MGT load. Operating at base load, the best fuel economy of 4.5 l/100 km is achieved which corresponds to a range of 890 km. However, at base load, the maximum and final NO_X emissions of 112 mg/km and 86 mg/km respectively, surpass the regulatory limit. Fully compliant emissions are only achieved at 25 kW MGT load and below. CO decreases from 217 mg/km to 26 mg/km between 10 kW and 30 kW MGT load. In light of possibly stricter limits for EURO 7 regulations, operation in this driving scenario might even be limited to a single operation point at 15 kW with regard to NO_X and CO emissions.

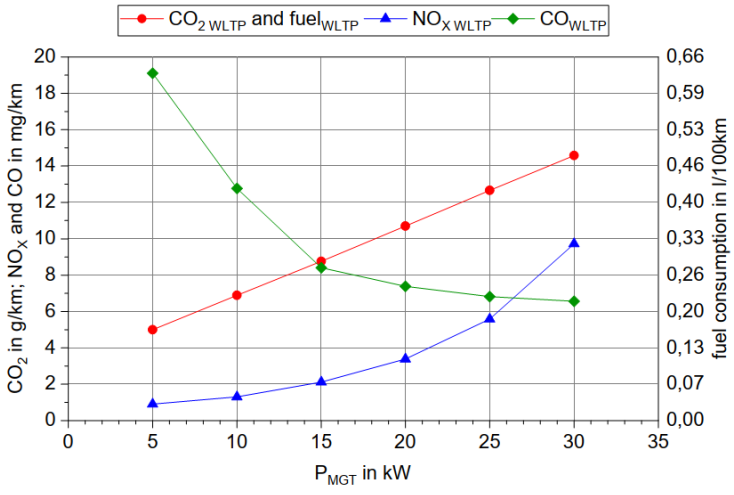

Figure 10: Range and emission results for the WLTP test with constant load OPC (A) dependent on MGT load setpoint

As can be seen in Figure 10, the WLTP test does not exhibit the aforementioned behavior at 5 kW MGT load. The battery capacity is sufficient to supply the vehicle during the CS cycle. NO_X and CO emissions show a similar dependency on MGT load as for the full range test, but with significantly lower magnitude due to the UF. NO_X emissions lie between 0.9 mg/km and 9.7 mg/km, CO between 19.1 mg/km and 6.6 mg/km. One particular difference are the CO_2 emissions. While they decrease with higher MGT loads during the full range test, they increase for the WLTP test. This seems surprising since higher CO_2 emissions indicate a lower fuel efficiency. Figure 4, however, shows that MGT efficiency increases with MGT load. This inversion of the trend for the WLTP is explained by the excess charge above the initial level (and subsequently excess fuel consumption) during the CS test for higher MGT loads. If the SOC is not just maintained but increased, the additional charge of the battery is not compensated for in form of a CO_2 reduction. Therefore, operation on overall more efficient, higher MGT loads results in a less efficient rating according to the WLTP. Despite this effect, operating the MGT in a fixed load set point already shows the high potential of this range extender system. WLTP emissions could satisfy even the strictest perspective of EURO 7 limitations. The maximum CO_2 emissions of 14.6 g/km, corresponding to a fuel consumption of less than 0.5 l/100 km, are also beneficial for manufacturers' fleet statistics. However, the comparably high NO_X emissions during the full range test while operating the MGT at base load necessitate considering more flexible OPCs.

Load Following Operation (B)

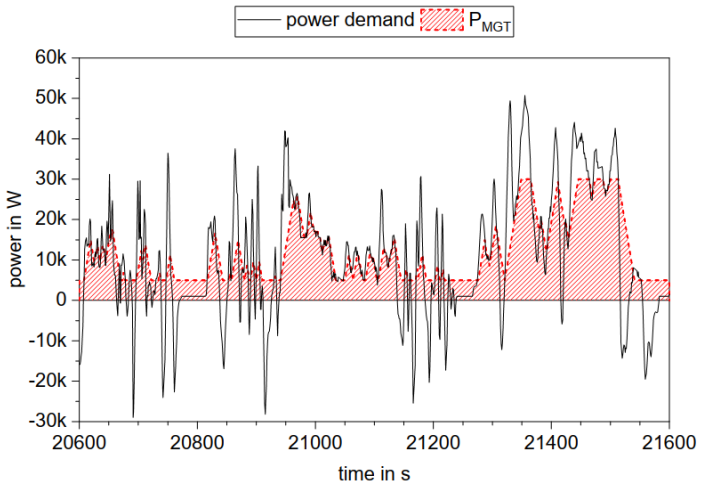

Figure 11: Excerpt of the WLTC power profiles for load following operation OPC (B) between 5 kW and 30 kW

Figure 11 shows the load profiles during a section of the WLTC with the MGT operating in load following mode between 5 kW and 30 kW. The black line shows the power demand (and recuperation) of the traction engine and auxiliaries in comparison to the power provided by the MGT as shaded area. The high gradients and strong peaks required by the velocity profile are significantly smoothed by the maximum load gradient and power limitations of the MGT.

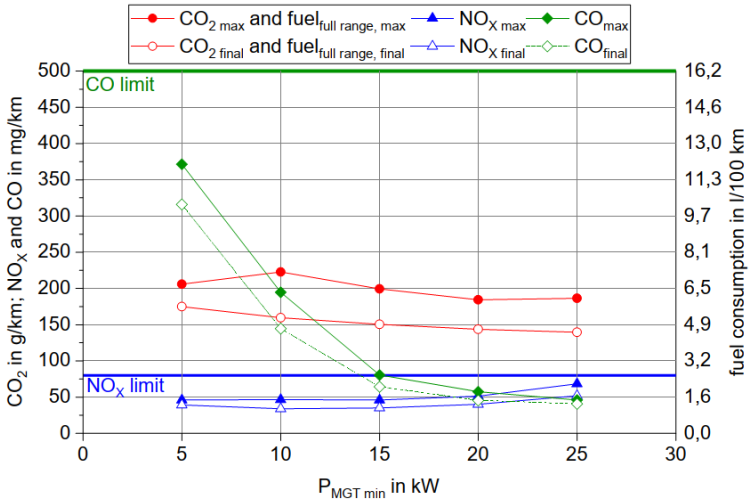

Figure 12: Range and emission results for the full range test with load following OPC (B) dependent on the lower MGT load limit

The emission and fuel consumption trends are shown in Figure 12; they are consistent to the behavior of the constant load OPC (A) (Figure 9). Additionally, it can be seen that emission compliance is maintained in all cases for NO_X and CO during the entire test, while also achieving a minimum fuel consumption of 4.55 l/100 km, corresponding to range of up to 889 km. Hence CO_2 emissions vary around 150 g/km. NO_X varies between 33.8 mg/km and 51.9 mg/km with the minimum situated at a load variation down to 10 kW. CO emissions can be reduced from 316 mg/km to 41 mg/km by increasing the lower load boundary from 5 kW to 25 kW.

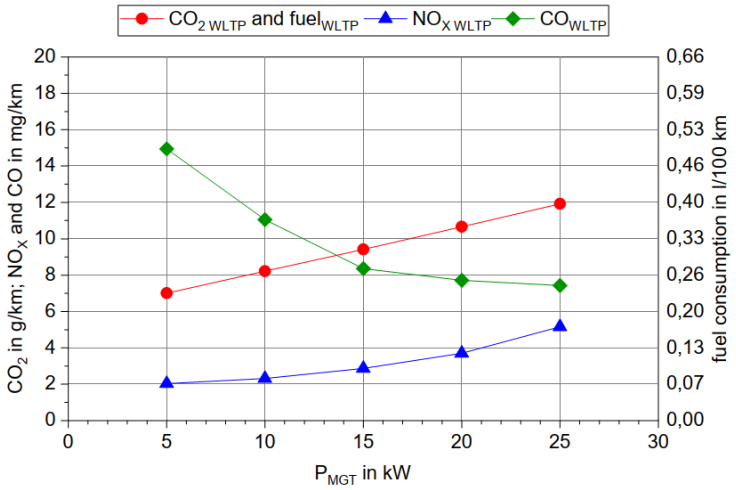

Figure 13: Range and emission results for the WLTP test with load following (B) dependent on the lower MGT load limit

OPC (B) also exhibits very low emission values in the WLTP test, as shown in Figure 13. If the lower MGT load limit is increased from 5 kW to 25 kW, NO_X emissions increase from 2.0 mg/km to 5.1 mg/km and CO drops from 15.0 mg/km to 7.4 mg/km. Because the OPC has less variability for higher MGT load limits and hence the batteries will be further charged than required, CO_2 emissions again show an inverted trend rising from 7.0 g/km to 11.9 g/km corresponding to a fuel consumption between 0.23 l/100 km and 0.39 l/100 km.

In light of the promising results of the load following OPC, it has to be considered that MGTs are optimized for steady state operation and that emissions increase during transient maneuvers. Figure 14 shows fuel consumption and emissions for load changes of 15 kW steps, as measured by [19]. It can be seen that, after a load-increase (a)) is initialized, CO emissions spike up 5 ppm during 5 s and NO_X emissions are slightly increased during the first 30 s before stabilizing. During a load reduction (b)) it can especially be observed that CO

emissions are elevated for about 80 s. Capturing these effects would have significantly increased the complexity of the vehicle model in this study. Therefore, it has to be considered that for operation strategies with a large number of load-changes the model under-predicts the actual emission masses.

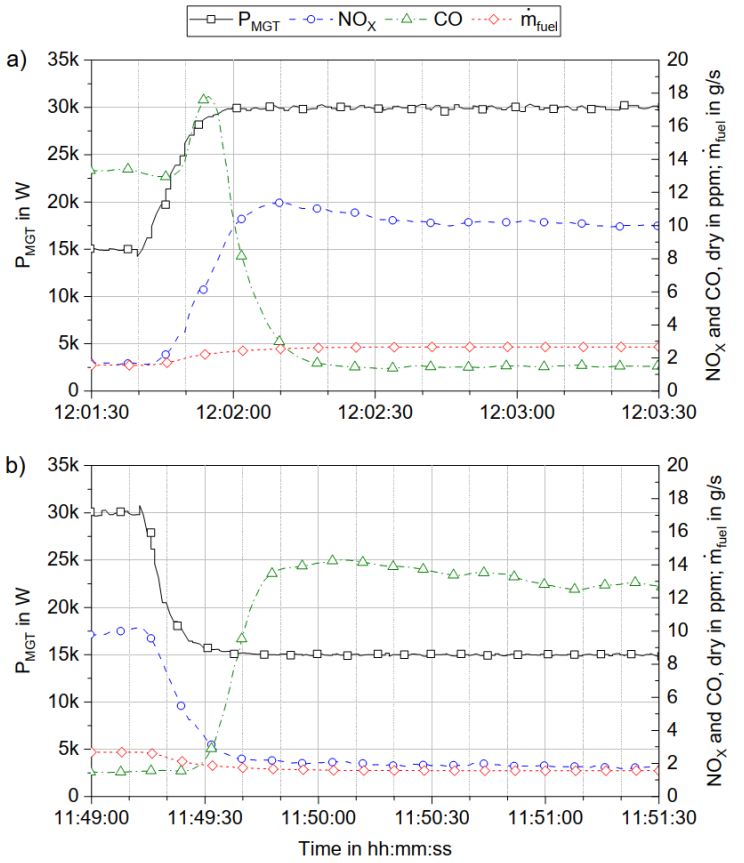

Figure 14: Transient emissions and fuel consumption for MGT loading a) and deloading b)

SOC and Power Consumption Dependent Operation (C)

As a compromise between OPC (A) and (C), this operation concept will maintain a constant load but adapt the set-point depending on the SOC of the battery and the current power demand as shown in Figure 6, hence still offering a wide range of variability (s. Table 6).

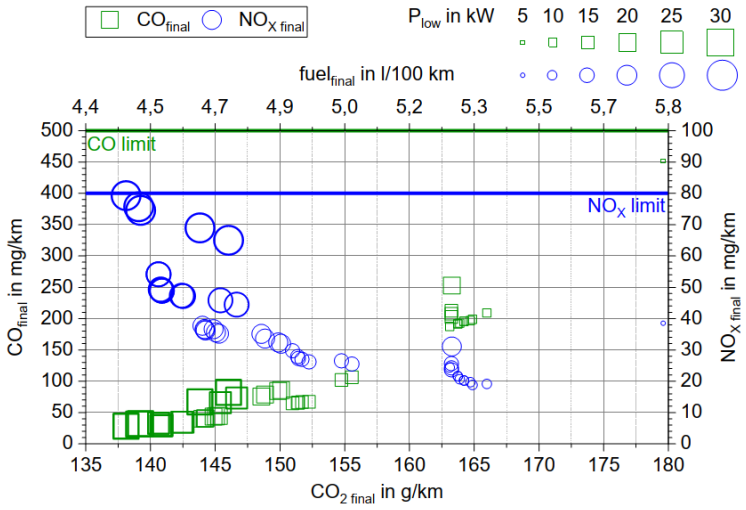

Figure 15: Range and emission results for the full range test with SOC and power demand OPC (C) dependent on CO_2 and P_{min} (Table 6)

Due to the number of variables, the results cannot be pinned down to the variation of a single parameter. Therefore, Figure 15 shows the NO_X and CO results of OPC (C) as function of CO_2. It can be seen that the final emission values are below the regulatory NO_X and CO limits. Also, most of the maximum emission masses that occur during the full range test remain well below the limits. Only for tests with final NO_X readings above 60 mg/km, the maximum values (not shown in Figure 15) exceed the limit during the test (Table 6, Indices 28, 44, 45). A mark of distinction in the results constitutes the P_{low} set point of the MGT which is bubble-size coded in Figure 15. The graph shows that CO_2 and CO emissions can be reduced from 180 g/km to 138 g/km and 451 mg/km to 28 mg/km respectively, with higher P_{low} set points. However, at the expense of higher NO_X emissions which increase from 19 mg/km to 79 mg/km. The simulations with a P_{low} set point of 15 kW and 20 kW and a fuel consumption between 4.5 l/100 km and 5 l/100 km show the most promising trade-off.

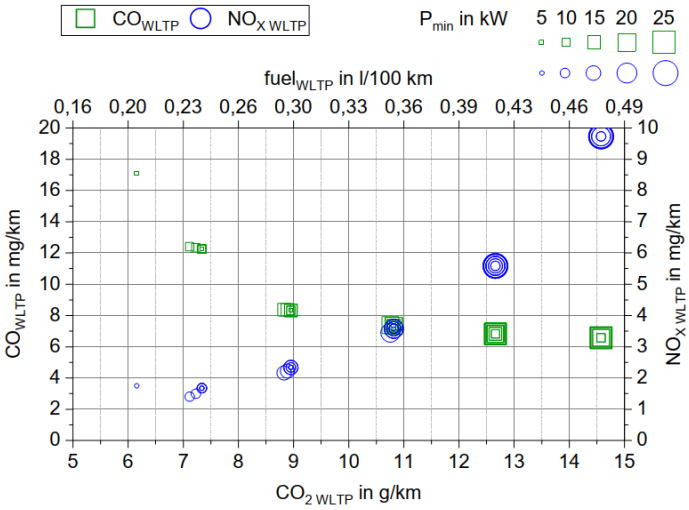

Figure 16: Range and emission results for the WLTP test with SOC and power demand OPC (C) dependent on CO_2 and P_{min} (Table 6)

The results of the WLTP evaluation follow the trend with inverted dependencies as already discussed in the previous sections. A clustering of the results becomes apparent in Figure 16. It can be shown that the six clusters only depend on the P_{low} set point, with 25 kW yielding the lowest CO_2 emissions and 5 kW the highest. As the CS cycle is carried out with a depleted battery, only the low SOC trunk of the decision tree (Figure 6) is relevant. During the CS cycle, for most of the OPC combinations, it only happens for short periods of time that power demand exceeds power supply of the MGT, hence the P_{low} set point is active most of the time. For higher P_{low} set point, the clusters can be subdivided, with respect to the P_{min} set point, indicated in Figure 16 by the size of the marks. With increasing P_{min}, NO_X and CO_2 decrease and CO increases. Due to the UF, emissions overall remain at a very low level. CO_2 emissions range from 6.2 g/km to 14.6 g/km, corresponding to less than 0.5 l/100 km fuel consumption. CO lies between 6.6 mg/km and 17.1 mg/km and NO_X between 1.4 mg/km and 9.7 mg/km.

The results of OPC (C) are very promising, WLTP emissions are similarly low as the previous OPCs. Further, emission limits are easily met during the full range test for a wide range of configurations, while the amount of MGT load changes is significantly reduced.

Influence of Battery Capacity

The UF only depends on the pure electric range of the vehicle which is mostly independent of the utilized range extender. Due to the significant differences between the results of the full range test, which are not UF corrected, and those of the WLTP test, it is worth taking a look at the influence of the UF. Main driver of the pure electric range, and in consequence the UF, is the battery capacity C_{bat}, which is now varied between 9.5 kWh and 47.5 kWh for the cases of OPC (A). The UFs, resulting from the different battery capacities, are shown in Table 7.

Table 7: Utility Factor dependent on battery capacity C_{bat}

C_{bat}	47.5	38	28.5	19	9.5	kWh
UF	0.98	0.97	0.96	0.92	0.84	-

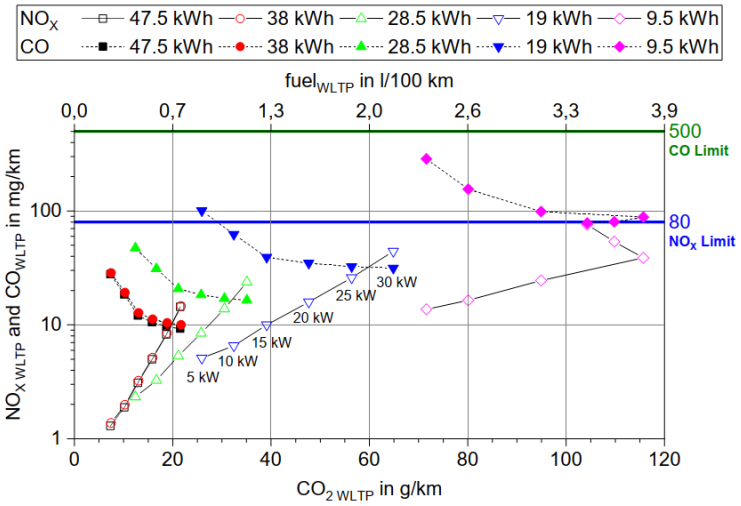

Figure 17: WLTP emission results for constant load OPC with different load setpoints for varying battery capacity

Figure 17 shows the WLTP emission results for MGT load set points between 5 kW and 30 kW in 5 kW steps from left to right. Each set of graphs represents a different C_{bat}. As expected from the decreasing UF, it can be seen that all emission parameters (NO_X, CO and CO_2) increase for lower C_{bat}. Between 47.5 kWh and 38 kWh, the influence is negligible but becomes quite significant towards 9.5 kWh, which is close to the range of current Plug-In HEV with ICE. In all cases, the emissions remain below the regulatory limits. The trends for the lowest capacity of 9.5 kWh show an irregularity of decreasing CO_2 emissions for higher MGT load set points. This results from the battery reaching a *SOC* of 80 % before the end of the CS cycle and the MGT shutting down. Additionally, which is not visible in the graphs, battery capacities of 9.5 kWh and 19 kWh require an MGT load of more than 10 kW to complete the transition cycle of the CD test. Otherwise, *SOC* reaches 10 % before the cycle is concluded and the test is aborted. In a similar manner, the CS cycle cannot be completed for battery capacities of 28.5 kWh and below in combination with an MGT load set point of 5 kW. If CO_2 emissions of this variation are compared to current Plug-In HEV, which are in the range of 30 g/km, a battery capacity of 28.5 kWh would be required for a constant load OPC at maximum load. This is about twice the capacity of current Plug-In HEV. However, if the additional battery capacity can be traded for the potential weight savings of the MGT, the MGT REX brings the advantage of a strongly increased pure electric range alongside significantly lower CO and NO_X emissions [26] without exhaust after treatment, at CO_2 emission levels of current Plug-In HEV [27].

Summary and Conclusion

In this study, a vehicle simulator is developed and used to investigate the emission performance of a hybrid electric vehicle with a micro gas turbine-based range extender in the WLTP scenario. The vehicle simulator includes an in-detail modeling of the MGT's fuel consumption and emission behavior for steady state operation and transient maneuvers based on look up tables. The LUT data is derived from experimental measurement data of a 30 kW MGT.

The influence of three different MGT operation concepts (constant load, load following, *SOC* and traction demand dependent) is investigated according to the methods described in the WLTP, and further according to a driving scenario based on the WLTC but exploiting the maximum range given by the vehicle's battery and fuel capacity. It is shown that CO_2, CO and NO_X emissions correlate depending on the OPC and evaluation method. In most simulation cases, emissions are significantly below the EURO 6d limits. NO_X emissions tend to become

the limiting factor for OPCs with higher MGT load set points and CO emissions for lower load set points. With single digit NO_X emissions, CO below 20 mg/km and fuel consumptions below 0.5 l/100 km, the evaluation according to the WLTP yields results about an order of magnitude lower than the full range test. The WLTP results benefit greatly from the high utility factor of the chosen car platform. Therefore, the influence of different battery capacities is also investigated. If the potential weight savings from the application of an MGT range extender instead of piston-engine-based range extender can be translated into additional battery capacity, the lower MGT efficiency compared to piston engines can be compensated by the increased utility factor in the WLTP. Further the MGT range extender offers significantly lower CO and NO_X emissions without the requirement of exhaust gas after treatment.

Acknowledgements

Thanks to J. Roth for the support during the experiments that serve as basis for this simulator and to S. Sigle and C. David for providing the boundary conditions of the DLR NGC Inter Urban Vehicle.

ReferencesReferences

[1] German Environment Agency, Federal Ministry for Environment, Nature Conservation, and Nuclear Safety, "2019 greenhouse gas emissions in Germany declined by 6.3 percent: Energy sector slashes emissions, growth in building and transport sectors," 2020.

[2] Degrauewe, B., Pisoni, E., Peduzzi, E., Meij, A. de et al., "Urban NO2 Atlas," EUR, vol. 29943, Publications Office of the European Union, Luxembourg, ISBN 978-92-76-10386-8, 2019.

[3] Pearre, N.S., Kempton, W., Guensler, R.L., and Elango, V.V., "Electric vehicles: How much range is required for a day's driving?," *Transportation Research Part C: Emerging Technologies* 19(6):1171–1184, 2011, doi:10.1016/j.trc.2010.12.010.

[4] Fischer, R., Fraidl, G.K., Hubmann, C., Kapus, P.E. et al., "Range extender module - Enabler for electric mobility," *MTZ worldwide* 70(10):38–44, 2009, doi:10.1007/BF03227981.

[5] Mackay, R., "Development of a 24 kW Gas Turbine-Driven Generator Set for Hybrid Vehicles," *SAE Technical Papers*(940510):99–105, 1994, doi:10.4271/940510.

[6] Leontopoulos, C., Etemad, M.R., Pullen, K.R., and Lamperth, M.U., "Hybrid vehicle simulation for a turbogenerator-based power-train," *Proceedings of the Institution of Mechanical Engineers, Part D: Journal of Automobile Engineering* 212(5):357–368, 1998, doi:10.1243/0954407981526028.

[7] Capata, R. and Sciubba, E., "The concept of the gas turbine-based hybrid vehicle: system, design and configuration issues," *International Journal of Energy Research* 30(9):671–684, 2006, doi:10.1002/er.1178.

[8] Capata, R., "Implementing a Hybrid Series Bus with Gas Turbine Device - A Preliminary Study," *International Journal of Advanced Engineering Research and Science (IJAERS)* June 2016(3):135–143, 2016.

[9] Arefin, M.A. and Mostakim, K., "Micro gas turbine for range extender electric vehicle: development of numerical model for investigating some validation parameters," *International Journal of Sustainable Engineering* 13(5):327–336, 2020, doi:10.1080/19397038.2020.1773566.

[10] Chen, J., Mitchell, M.G., and Nourse, J.G., "Development of Ultra-low Emission Diesel Fuel-fired Microturbine Engines for Vehicular Heavy Duty Applications: Combustion Modifications," *Proceedings of ASME Turbo Expo 2010, Glasgow, UK*, 2010.

[11] Christodoulou, F., Giannakakis, P., and Kalfas Anestis I., "Performance Benefits of a Portable Hybrid Micro-Gas Turbine Power System for Automotive Applications," *ASME Journal of Engineering for Gas Turbines and Power* 133(2):22301, 2011, doi:10.1115/1.4002041.

[12] Karvountzis-Kontakiotis, A., Andwari, A.M., Pesyridis, A., Russo, S. et al., "Application of Micro Gas Turbine in Range-Extended Electric Vehicles," *Energy* 147:351–361, 2018, doi:10.1016/j.energy.2018.01.051.

[13] Shah, R., McGordon, A., Amor-Segan, M., and Jennings, P., "Micro Gas Turbine Range Extender - Validation Techniques for Automotive Applications," in: IET (ed.), *Proceedings of the 2013 IET Hybrid and Electric Vehicles Conference*: London, UK, 1–6, 2013.

[14] Shah, Raja Mazuir Raja Ahsan, Qubeissi, M.A., McGordon, A., Amor-Segan, M. et al., “Micro Gas Turbine Range Extender Performance Analysis Using Varying Intake Temperature,” *Automotive Innovation* 3(4):356–365, 2020, doi:10.1007/s42154-020-00119-9.

[15] Shah, Raja Mazuir Raja Ahsan, McGordon, A., Rahman, M.M., Amor-Segan, M. et al., “Characterisation of micro turbine generator as a range extender using an automotive drive cycle for series hybrid electric vehicle application,” *Applied Thermal Engineering* 184:116302, 2021, doi:10.1016/j.applthermaleng.2020.116302.

[16] European Union, “Commission Regulation (EU) 2017/1151 - Worldwide harmonised Light-duty vehicles Test Procedure (WLTP) and Real Driving Emissions (RDE),” *Official Journal of the European Union* L 175(260), 2017.

[17] David, C. and Vohrer, S., “Development of novel vehicle structures for automotive series production,” *Proceedings of 18. Internationales Stuttgarter Symposium Automobil- und Motorentechnik*, Stuttgart, Germany, 2018.

[18] Capstone Turbine Company, “Products - C30 - Solutions,” 2021.

[19] Kislat, O., Zanger, J., Krummrein, T., Kutne, P. et al., “Detailed Experimental Investigation of the Operational Parameters of a 30 kW Micro Gas Turbine,” *Proceedings of ASME Turbo Expo 2019, Pheonix, AZ, USA*, New York, N.Y., 2019.

[20] Guzzella, L. and Sciarretta, A., “Vehicle propulsion systems: Introduction to modeling and optimization,” 2nd ed., Springer, Berlin, ISBN 978-3-540-74691-1, 2007.

[21] Guttenberg, P., “Der Autarke Hybrid am Prüfstand – Funktion, Kraftstoffverbrauch und energetische Analyse,” TU München, 2004.

[22] Helms, H., Pehnt, M., Lambrecht, U., and Liebich, A., “Electric vehicle and plug-in hybrid energy efficiency and life cycle emissions,” *Proceedings of 18th International Symposium Transport and Air Pollution*, Zurich, Switzerland, 2010.

[23] Mansour, C., Bou Nader, W., Breque, F., Haddad, M. et al., “Assessing additional fuel consumption from cabin thermal comfort and auxiliary needs on the worldwide harmonized light vehicles test cycle,” *Transportation Research Part D: Transport and Environment* 62:139–151, 2018, doi:10.1016/j.trd.2018.02.012.

[24] European Union, “Commission Regulation (EU) No 459/2012 amending Regulation (EC) No 715/2007 of the European Parliament and of the Council and Commission Regulation (EC) No 692/2008 as regards emissions from light passenger and commercial vehicles (Euro 6),” *Official Journal of the European Union* L 142(16):16–24, 2012.

[25] Samaras, Z. and Hausberger, S., “Preliminary findings on possible Euro 7 emission limits for passenger cars and LCVs,” *Online AGVES Meeting*(21.10.2020), 2020.

[26] Deutsche Energie Agentur, “NOx-Emissionen unterschiedlicher Antriebsarten,” 2019.

[27] GreenGear.de, “Marktübersicht: Plug-In-Hybridautos (PHEV) - Liste der Plug-In-Hybrid-Neuwagen im Jahr 2021,” 2021.

Appendix A: Simulation Cycle